20. Magara, F. *et al.* Genetic background changes the pattern of forebrain commissure defects in transgenic mice underexpressing the β-amyloid-precursor protein. *Proc. Natl Acad. Sci. USA* **96,** 4656–4661 (1999).
21. Ferreira, A., Niclas, J., Vale, R. D., Banker, G. & Kosik, K. S. Suppression of kinesin expression in cultured hippocampal neurons using antisense oligonucleotides. *J. Cell Biol.* **117,** 595–606 (1992).
22. Okada, Y., Yamazaki, H., Sekine-Aizawa, Y. & Hirokawa, N. The neuron-specific kinesin superfamily protein KIF1A is a unique monomeric motor for anterograde axonal transport of synaptic vesicle precursors. *Cell* **81,** 769–780 (1995).
23. Otsuka, A. J. *et al.* The *C. elegans unc-104* gene encodes a putative kinesin heavy chain-like protein. *Neuron* **6,** 113–122 (1991).
24. Potempska, A., Styles, J., Mehta, P., Kim, K. S. & Miller, D. L. Purification and tissue level of the β-amyloid peptide precursor of rat brain. *J. Biol. Chem.* **266,** 8464–8469 (1991).
25. Hollenbeck, P. J. The distribution, abundance and subcellular localization of kinesin. *J. Cell Biol.* **108,** 2335–2342 (1989).
26. Xia, W. *et al.* Presenilin complexes with the C-terminal fragments of amyloid precursor protein at the sites of amyloid β-protein generation. *Proc. Natl Acad. Sci. USA* **97,** 9299–9304 (2000).
27. Bowman, A. B. *et al.* Kinesin-dependent axonal transport is mediated by the Sunday driver (SYD) protein. *Cell* **103,** 583–594 (2000).
28. Verhey, K. J. *et al.* Cargo of kinesin identified as JIP scaffolding proteins and associated signaling molecules. *J. Cell Biol.* **152,** 959–970 (2001).
29. Kim, S. H., Lah, J. J., Thinakaran, G., Levey, A. & Sisodia, S. S. Subcellular localization of presenilins: association with a unique membrane pool in cultured cells. *Neurobiol Dis.* **7,** 99–117 (2000).
30. Cao, X. & Sudhof, T. C. A transcriptively active complex of APP with Fe65 and histone acetyltransferase Tip60. *Science* **293,** 115–120 (2001).

Supplementary Information accompanies the paper on *Nature*'s website (http://www.nature.com).

Acknowledgements

We thank G. Stokin for the Kif5b antibody, S. Brady for the 63-90 Klc antibody, S. Sisodia for providing the Ps1, Aplp1 and Aplp2 antibodies, and Merck for the APP-null mice. We thank D. Cleveland for discussions, and S. Emr for use of the deconvolution microscope. This work is supported by a grant from the National Institutes for Health. L.S.B.G. is an investigator of the Howard Hughes Medical Institute.

Correspondence and requests for materials should be addressed to L.S.B.G. (e-mail: lgoldstein@ucsd.edu).

Group A *Streptococcus* tissue invasion by CD44-mediated cell signalling

Colette Cywes* & Michael R. Wessels*†

** Channing Laboratory, Brigham and Women's Hospital and † Division of Infectious Diseases, Children's Hospital, Harvard Medical School, Boston, Massachusetts 02115, USA*

***Streptococcus pyogenes* (also known as group A *Streptococcus*, GAS), the agent of streptococcal sore throat and invasive soft-tissue infections, attaches to human pharyngeal or skin epithelial cells through specific recognition of its hyaluronic acid capsular polysaccharide by the hyaluronic-acid-binding protein CD44 (refs 1, 2). Because ligation of CD44 by hyaluronic acid can induce epithelial cell movement on extracellular matrix[3–5], we investigated whether molecular mimicry by the GAS hyaluronic acid capsule might induce similar cellular responses. Here we show that CD44-dependent GAS binding to polarized monolayers of human keratinocytes induced marked cytoskeletal rearrangements manifested by membrane ruffling and disruption of intercellular junctions. Transduction of the signal induced by GAS binding to CD44 on the keratinocyte surface involved Rac1 and the cytoskeleton linker protein ezrin, as well as tyrosine phosphorylation of cellular proteins. Studies of bacterial translocation in two models of human skin indicated that cell signalling triggered by interaction of the GAS capsule with CD44 opened intercellular junctions and promoted tissue penetration by GAS through a paracellular route. These results support a model of host cytoskeleton manipulation and tissue invasion by an extracellular bacterial pathogen.**

To investigate the ability of GAS to affect host epithelial cell biology, we studied the interaction of GAS with human keratinocytes—the predominant cell type in skin and the pharyngeal epithelium. Keratinocytes were grown to confluence on porous membrane supports under conditions that induced both the physiological apical–basal polarization of the epithelial cells and the formation of intercellular junctions[6,7]. These confluent, differentiated cell cultures are referred to hereafter as monolayers, although microscopy showed partial overlap of adjacent cells so that the thickness of the layer in an individual well varied from 1 to 3 cells (see Fig. 1). Monolayers were inoculated by placement of a suspension of GAS on the apical surface of the cells. Transmission electron microscopy images showed membrane projections from keratinocytes that were exposed to wild-type GAS strain 950771, but not from cells exposed to an isogenic acapsular mutant, strain 188 (Fig. 1a). Similar membrane ruffles or lamellipodia have been observed in response to localized application of hyaluronic acid to the surface of tumour cells as a consequence of CD44-mediated cell signalling[4].

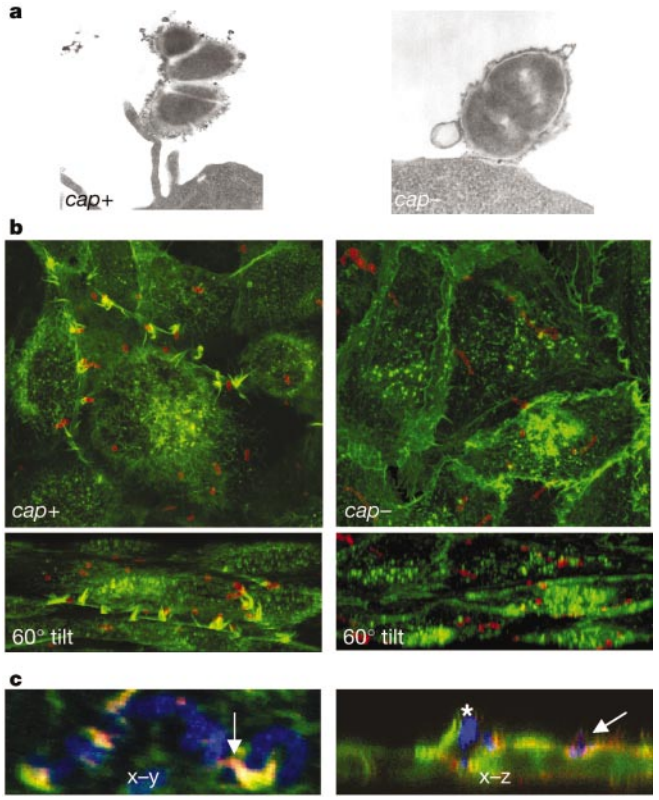

Figure 1 Induction of lamellipodia formation by GAS binding to keratinocytes. **a**, Transmission electron microscopy images showing binding of wild-type GAS (*cap*+) to membrane projections or lamellipodia of keratinocytes. Binding of the acapsular mutant strain (*cap*–) is not associated with lamellipodia formation (original magnification, 30,000×). **b**, Confocal microscopy images of GAS (red) interaction with polarized keratinocyte monolayers. Wild-type (*cap*+), but not acapsular (*cap*–), GAS are closely associated with actin (labelled green) filament projections, seen in the 60° tilt view to extend up from the plane of the monolayer (original magnification, 100×). **c**, Confocal microscopy images of interaction of wild-type GAS (blue) with polarized keratinocyte monolayers. Co-localization of actin (green) and CD44 (red) appears as yellow staining. CD44 is seen along intercellular junctions and at the tips of actin filament projections in close association with GAS (arrow in x–y panel, original magnification, 200×). The vertical section (x–z panel, original magnification, 150×) demonstrates association of GAS with CD44 on the keratinocyte surface (arrow), and lifting of the edge of a cell with closely associated GAS seen within the intercellular gap (asterisk).

In confocal microscopy images of monolayers exposed to wild-type GAS, we observed actin filament projections in close association with the bacteria (Fig. 1b). Triple-label experiments in which CD44 was visualized with specific antibody demonstrated that CD44 was distributed along intercellular junctions and at the tips of the actin filament projections, immediately adjacent to bound GAS (Fig. 1c). These microfilament projections were not observed in keratinocytes that were pretreated with anti-CD44 monoclonal antibody IM7.8.1 before inoculation with wild-type GAS, nor in untreated keratinocytes exposed to acapsular GAS. Furthermore, cell-bound acapsular bacteria were not colocalized with CD44.

In tumour cells, transduction of the extracellular event of hyaluronic acid binding to CD44 to the intracellular movement of actin filaments occurs through activation of Rac1, a member of the Rho family of small GTPases[4,8]. To determine whether Rac1 was involved in CD44-mediated cell signalling induced by GAS, we transfected keratinocytes with N17Rac1 (dominant negative Rac1). Binding of wild-type GAS to cells transfected with N17Rac1 failed to induce formation of lamellipodia, although typical lamellipodia were induced by interaction of GAS with adjacent untransfected cells in the same keratinocyte monolayer (Fig. 2). Transfection of keratinocytes with constitutively active L61Rac1 resulted in the formation of lamellipodia in uninoculated keratinocytes. Inoculation of these cells with wild-type GAS increased the amount of lamellipodia, and wild-type GAS was observed in close association with the lamellipodia. However, binding of acapsular GAS to keratatinocytes transfected with L61Rac1 was not preferentially localized to lamellipodia, but rather occurred equally over regions of the cell that were devoid of membrane projections. These results demonstrate an absolute requirement for active Rac1 in the cytoskeletal rearrangements induced by wild-type GAS.

CD44-mediated cell signalling to the cytoskeleton in other systems additionally involves ezrin, a protein of the ezrin–radixin–moesin (ERM) family, which is thought to physically link the cytoplasmic domain of CD44 to the actin cytoskeleton on activation[9–11]. In keratinocytes that were exposed to wild-type GAS, confocal microscopy demonstrated colocalization of Rac1 and ezrin precisely at the point of attachment of GAS to the keratinocyte surface (Supplementary Information Fig. 1a, b). By contrast, binding of acapsular GAS to keratinocytes was not associated with co-localization of Rac1 and ezrin with the bound bacteria. These results support the hypothesis that binding of the GAS hyaluronic acid capsule to keratinocyte CD44 triggers the local activation of Rac1 and association of the actin linker protein ezrin with the cytoplasmic domain of CD44. This process physically couples the keratinocyte cell membrane, by means of CD44 and ezrin, to the actin cytoskeleton. Thus, Rac1-mediated actin polymerization could result in local movement of the cell membrane to form lamellipodia and, potentially, to open intercellular junctions with neighbouring cells (see below).

Ligand binding to CD44 is expected to activate cellular protein tyrosine kinases as part of the downstream intracellular signalling cascade[5,12]. Consistent with this model, at the site of attachment of wild-type, but not acapsular, GAS to the keratinocyte surface, confocal microscopy revealed co-localization of antibody to tyrosine-phosphorylated protein(s) with CD44 (Supplementary Information Fig. 1c). We also found that incubation of keratinocytes with the protein tyrosine kinase inhibitor, genistein, inhibited formation of lamellipodia in response to GAS, evidence that tyrosine phosphorylation of an as yet unidentified protein may serve to couple CD44 signalling to Rac1 activation.

Scanning electron microscopy and confocal microscopy images of keratinocyte monolayers that were exposed to GAS showed not only evidence of localized membrane projections, but also lifting of the margin of the keratinocyte near associated GAS, with curling back of the cell membrane from its contacts with the subtratum and with the neighbouring cell (Fig. 3a). Similar morphological changes have been observed in epithelial cells subjected to localized application of hyaluronic acid or to microinjection with constitutively active Rac1 (refs 4, 11). In several instances GAS organisms were observed, below the surface of the monolayer, within the intercellular breach (see, for example, Fig. 1c). Such disruptions of intercellular junctions were not observed in keratinocytes that were exposed to acapsular GAS. We investigated whether GAS-induced disruption of intercellular junctions was associated with changes in distribution of the tight junction protein, zonula occludens-1 (ZO-1) or of E-cadherin—a member of the cadherin family of transmembrane proteins that mediate cell–cell adhesion through homophilic interaction of their extracellular domains on adjacent cells. Immunofluorescent staining demonstrated marked

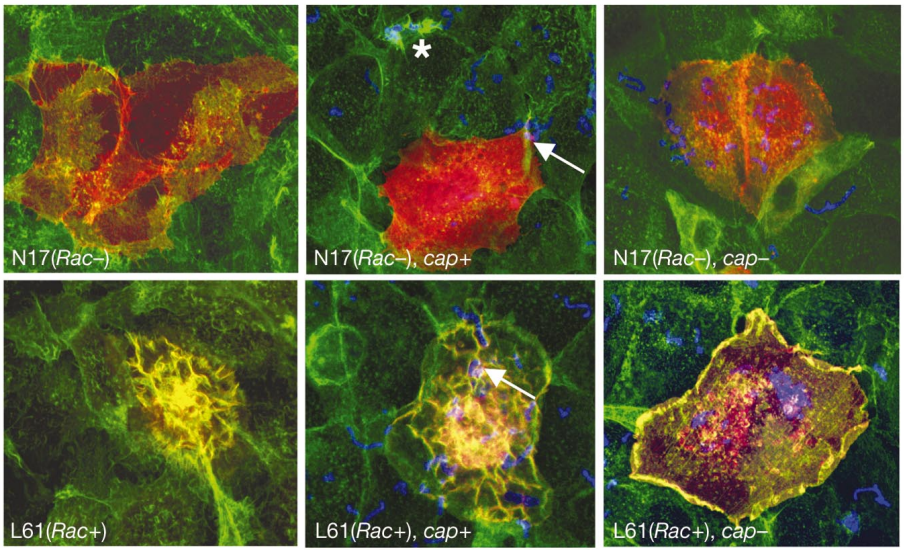

Figure 2 Confocal microscopy images of GAS interaction with keratinocytes expressing dominant negative (N17) or constitutively active (L61) Rac1. Samples were stained with antibody to the Myc tag (red) to identify transfected cells, with phalloidin (green) to label the cytoskeleton and with antibody to identify GAS (blue). Wild-type GAS (*cap*+) failed to trigger lamellipodia formation in cells transfected with N17Rac (arrow in the middle panel of the top row), although GAS organisms were associated with lamellipodia in untransfected cells in the same monolayer (asterisk). Cells transfected with L61Rac produced abundant lamellipodia that co-localized with wild-type GAS (arrow in the middle panel of the bottom row), but not with acapsular GAS (*cap*–; bottom right panel (original magnification, 100×).

loss of both ZO-1 (Fig. 3b) and E-cadherin (not shown) from intercellular junctions after exposure of keratinocytes to wild-type, but not acapsular, GAS. This redistribution was prevented by pretreatment of the keratinocytes with genistein, implicating tyrosine kinase(s) in the process. These findings provide further evidence that interaction of the GAS hyaluronic acid capsule with CD44 results in Rac1-dependent disruption of intercellular junctions. Loss of integrity of intercellular junctions is expected to reduce the barrier function of the monolayer, as reflected by its ability to prevent the passage of small molecules such as sodium fluorescein. Infection of monolayers with the encapsulated wild-type strain resulted in an increase in permeability to sodium fluorescein (from less than 3% to greater than 30%), and a corresponding 33% decrease in transepithelial electrical resistance after 6 h of exposure. However, infection with the acapsular mutant strain resulted in no significant change in the barrier function of the monolayer.

The finding that GAS binding to CD44 induced destabilization and opening of intercellular junctions suggested that these defects in epithelial integrity might facilitate translocation of the bacteria through the epithelium. As a model of the movement of GAS from the pharyngeal mucosa or skin surface into underlying tissue, we studied GAS translocation *in vitro* through keratinocyte monolayers. Two hours after inoculation onto the surface of a confluent keratinocyte monolayer, wild-type GAS could be detected in the culture medium below the membrane support, indicating migration of the bacteria through the monolayer. At each of several intervals after inoculation, approximately 20–100 times as many GAS colony-forming units were recovered below monolayers inoculated with wild-type GAS compared with those inoculated with the acapsular mutant strain (Fig. 4a). A comparable difference in efficiency of translocation between wild-type and acapsular GAS was observed in separate experiments using monolayers of primary human keratinocytes (data not shown). Compared to wild-type GAS strain 950771, the efficiency of translocation was similar for wild-type GAS strains 87-282, a highly encapsulated M-type 18 strain, and DLS003, a poorly encapsulated M-type 3 strain (data not

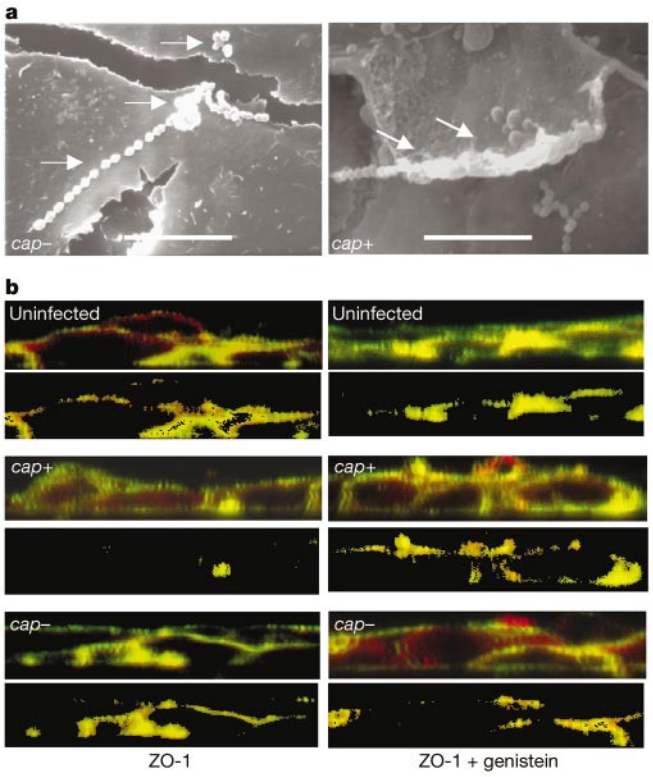

Figure 3 GAS-induced disruption of intercellular junctions. **a**, Scanning electron microscopy images of the interaction of GAS with polarized keratinocyte monolayers. Cells inoculated with wild-type strain (*cap*+), but not the acapsular strain (*cap*–), exhibit membrane ruffling and lifting and curling back of the edge of the cell around the associated GAS. The arrows indicate GAS. Scale bar, 10 μm. **b**, Confocal microscopy images demonstrating loss of ZO-1 from intercellular junctions on exposure of keratinocytes to wild-type (*cap*+), but not acapsular (*cap*–), GAS. Samples were stained with antibody to ZO-1 (red) and with phalloidin (green) to label the cytoskeleton. Images represent vertical sections (x–z plane) through keratinocyte monolayers. The bottom image of each pair shows co-localization of ZO-1 and actin (indicated by yellow staining). Pretreatment with genistein prevented redistribution of ZO-1 on exposure to GAS (original magnification, 100×).

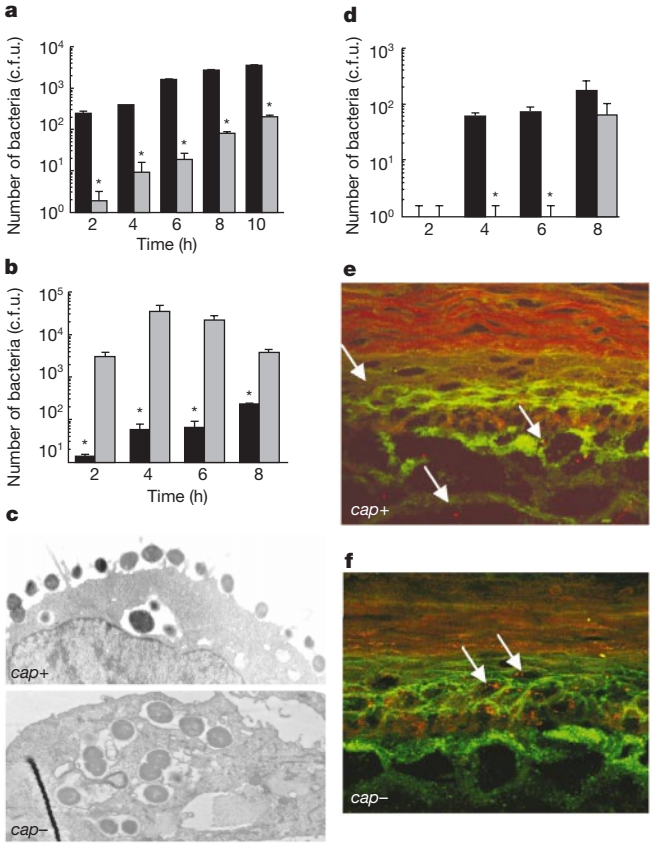

Figure 4 GAS translocation across model epithelia. **a**, Translocation of GAS through polarized keratinocyte monolayers. Data represent mean number of colony-forming units (c.f.u.) recovered from the medium beneath the monolayer at indicated times after inoculation of the apical surface with wild-type (black bars) or acapsular (grey bars) GAS. Asterisk, $P = 0.0002$ for comparison with the wild-type strain. **b**, Internalization of GAS by keratinocytes in a polarized monolayer. At indicated time points after inoculation of the apical surface of the monolayer, extracellular GAS was killed by addition of penicillin and gentamicin, and intracellular GAS was recovered after lysis of the keratinocytes. Data represent mean c.f.u. of intracellular GAS recovered from monolayers inoculated with wild-type (black bars) or acapsular (grey bars) GAS. Asterisk, $P = 0.0002$ for comparison with acapsular strain. **c**, Transmission electron microscopy images show wild-type GAS (*cap*+) associated with lamellipodia on the keratinocyte surface and a few organisms in spacious vacuoles within the cells; acapsular GAS (*cap*–) are visualized in large numbers intracellularly in membrane-bound vacuoles (original magnification, 6,500×). **d**, Translocation of GAS through human skin equivalent. Data represent mean number of c.f.u. of GAS recovered from beneath a sample of human skin equivalent (see text) at various times after inoculation of the epidermal surface with wild-type (black bars) or acapsular (grey bars) GAS. Asterisk, $P = 0.008$ for comparison with the wild-type strain. **e**, **f**, Confocal microscopy images of tissue sections of human skin equivalent 6 h after inoculation with wild-type (*cap*+) or acapsular (*cap*–) GAS. GAS organisms (indicated with arrows) are stained red and keratinocyte actin is stained green (original magnification, 100×).

shown). Translocation of wild-type GAS was reduced by 78% at 1 h in experiments in which the keratinocyte monolayers were pretreated with monoclonal antibody IM7.8.1 to block interaction of the GAS capsule with CD44. Similarly, in the presence of 250 μM genistein, the earliest detectable translocation of wild-type GAS, was delayed from 30 min to 1 h, and the maximum number of translocated GAS at 4 h was reduced by approximately 80% (data not shown).

Transmission electron microscopy showed wild-type GAS predominantly at extracellular sites (Fig. 4c). Organisms were seen on the apical surface of the cells in association with lamellipodia and in intercellular spaces. By contrast, organisms of the acapsular mutant strain that were visualized on the surface of keratinocytes appeared to be tightly apposed to the keratinocyte cell membrane and not associated with lamellipodia; furthermore, many acapsular bacteria were observed within keratinocytes in membrane-bound vacuoles (Fig. 4c). These results were confirmed by quantitative cultures of organisms recovered from cell lysates of infected keratinocytes. At 2 h after inoculation of the keratinocyte monolayer, approximately 200-fold more intracellular GAS organisms were recovered from monolayers infected with the acapsular mutant than from monolayers infected with the wild-type strain. Similar results were obtained in studies of monolayers infected for 4, 6 or 8 h (Fig. 4b). Thus, the efficiency of translocation through the monolayer was inversely related to entry of the bacteria into the keratinocytes. Trypan blue staining did not reveal large cytopathic changes in the keratinocytes during the period of the translocation assays. Furthermore, in assays measuring release of lactate dehydrogenase as a marker of cell injury, we found greater amounts of lactate dehydrogenase released from keratinocytes that were exposed to acapsular compared with wild-type GAS (C.C. and M.R.W., unpublished observations). Therefore, the increased translocation of wild-type compared with acapsular GAS cannot be attributed to a greater cytotoxic effect by the wild-type bacteria.

To examine GAS translocation in a model system similar to normal human skin, we used pseudo-organ cultures of human skin equivalent[13,14]. Histology of the human skin equivalent is very similar to that of normal human skin: a differentiated, stratified squamous epithelium that consists of multiple cell layers. As intact human skin is highly resistant to GAS infection, we simulated minor trauma to the superficial epidermis by abrading the surface of the skin equivalent with a cytology brush to introduce breaks in the stratum corneum. GAS organisms were inoculated onto the surface of abraded skin equivalent and translocation through the tissue was monitored at intervals by culture of GAS from the basal surface of the skin equivalent. Wild-type GAS was detected from the basal surface of the skin equivalent 4 h after surface inoculation, whereas acapsular GAS was not detected until 8 h after inoculation (Fig. 4d). Examination of histological sections by confocal microscopy revealed wild-type GAS in intercellular spaces throughout the epidermis and dermis, whereas acapsular GAS organisms were visualized primarily in the superficial layers of the epidermis, often within keratinocytes (Fig. 4e, f). Thus, capsule-deficient organisms fail to translocate efficiently, but rather remained trapped within keratinocytes in the superficial epidermis. These findings extend similar results obtained using keratinocyte monolayers to a system with important features of normal human skin.

Our results provide evidence for the following mechanism in bacterial pathogenesis: binding of the GAS hyaluronic acid capsule to CD44 on epithelial cells triggers cytoskeletal rearrangements that open intercellular junctions, thereby facilitating paracellular translocation of the organisms from the epithelial surface into underlying tissues. The CD44-mediated cell signalling events involve tyrosine phosphorylation of downstream effector proteins and the direct or indirect interaction of Rac1 and ezrin with the cytoplasmic domain of CD44. Organisms such as *Salmonella typhimurium* and *Shigella* spp. also elicit epithelial cell cytoskeletal rearrangements and membrane ruffling through activation of Rho family GTPases[15,16]. However, an important difference between GAS and Gram-negative enteric pathogens is the consequence of cytoskeletal rearrangements induced by bacterial contact with the host epithelial cell. In the epithelial cell response to *Salmonella* or *Shigella* spp., extension and subsequent fusion of lamellipodia entraps the bacteria and results in their internalization. By contrast, although interaction of GAS with CD44 produces marked membrane ruffling, subsequent internalization of wild-type (encapsulated) GAS is relatively inefficient, and most of the cell-associated bacteria remain extracellular. The predominant effect of CD44-mediated cytoskeletal rearrangements seems to be disruption of intercellular junctions to permit the passage between cells of GAS, which remain extracellular as they penetrate the epithelium. Thus, the hyaluronic acid capsule not only facilitates tissue invasion by disrupting intercellular junctions, but also by preventing internalization and trapping of the organisms within epithelial cells.

As the GAS strains that cause severe invasive infections such as necrotizing fasciitis do so only rarely—whereas pharyngitis caused by the same strains is common—it is clear that host factors are critical determinants in invasive disease. Nevertheless, the experimental observation that capsule-deficient mutants are avirulent in a mouse model of necrotizing fasciitis implies that capsule may be one of perhaps several bacterial factors that are required for invasive infection to occur[17]. Our findings support paracellular translocation as the mechanism of tissue invasion in such infections. Results of this study define a previously unknown virulence mechanism of a prototypic extracellular bacterial pathogen. □

Methods

Bacterial strains and polarized keratinocyte monolayers

The GAS strains that we used were 950771, an M-type 3 strain originally isolated from a child with necrotizing fasciitis, and 188, an isogenic acapsular mutant derived from 950771 (ref. 17). Bacteria were cultured in Todd Hewitt broth (Difco) to early exponential phase. For preparation of polarized keratinocyte monolayers, human squamous cell carcinoma cell line SCC13, derived from cheek epidermis[18], was cultured to confluence in serum-free keratinocyte medium (SFM, Gibco BRL) supplemented with 50 μg ml^{-1} bovine pituitary extract, 0.1 ng ml^{-1} epidermal growth factor and 0.3 mM calcium chloride (c-SFM). Certain experiments were performed using cell monolayers prepared from OKP7 primary human keratinocytes[19]. Keratinocytes were seeded at 5×10^5 cells per well onto polycarbonate Transwell membrane supports (12-well plates, 3.0-μm pore size; Costar) and cultured for 6–10 days at 37 °C with 5% CO_2 in c-SFM, with daily medium changes. Once confluent, the integrity of the monolayer was assessed routinely by measuring permeability to sodium fluorescein[20] and, in some experiments, by measuring transepithelial electrical resistance[21].

Antibody labelling and confocal microscopy

Keratinocyte monolayers were fixed with 4% paraformaldehyde in phosphate-buffered saline (PBS), washed, permeabilized with 0.1% Triton X-100 in PBS, then incubated with 0.5% bovine serum albumin (BSA) in PBS to block nonspecific binding sites before antibody staining. Primary antibodies included rabbit immunoglobulin-γ (IgG) antibody to GAS group A carbohydrate (ImmuCell) at 5 μg ml^{-1}, rat monoclonal anti-mouse CD44 (clone IM7.8.1)[1] at 15 μg ml^{-1}, goat IgG anti-ezrin at 2 μg ml^{-1} (Santa Cruz Biotechnology), goat IgG anti-Rac1 at 2 μg ml^{-1} (Santa Cruz Biotechnology), mouse anti-phosphotyrosine at 2 μg ml^{-1} (PY-Plus, Zymed Laboratories), rabbit anti-TJP1 at 2 μg ml^{-1} (Zymed), goat anti-E-cadherin at 2 μg ml^{-1} (Santa Cruz Biotechnology) and mouse anti-Myc monoclonal antibody 9E10 (Santa Cruz Biotechnology). Secondary antibodies included, as appropriate, Texas red- or Alexa 660-conjugated anti-rabbit IgG (Molecular Probes), Alexa 568-conjugated anti-rabbit, anti-goat, or anti-rat IgG (Molecular Probes) and fluorescein isothiocyanate-conjugated anti-goat or anti-mouse IgG (Sigma), each diluted 1:250 in 0.5% BSA/PBS. Cellular actin was labelled with 165 nm phalloidin conjugated to Oregon green 514 or to Alexa 488 (Molecular Probes).

Confocal microscopy images were collected using a BioRad scanning confocal microscope equipped with a krypton–argon laser. We processed images with BioRad Confocal Assistant and Adobe Photoshop 5.5 (Adobe Systems).

Transfection of SCC13 keratinocytes with Rac constructs

Eukaryotic expression plasmids pRK5-Myc-N17Rac1 (Myc-tagged, dominant negative Rac1) and pRK5-Myc-L61Rac1 (Myc-tagged, constitutively active Rac1) were provided by A. Hall. Polarized SCC13 keratinocyte monolayers were transiently transfected using 5 μg of either of the two expression constructs and 30 μl SuperFect transfection reagent (Qiagen). Twenty-four hours later the monolayers were inoculated with GAS as described below.

GAS translocation through polarized keratinocyte monolayers

Keratinocyte monolayers on Transwells were inoculated with GAS at a multiplicity of infection of 10 per keratinocyte. Monolayers were incubated at 37 °C with 5% CO_2. The keratinocyte medium in the upper chamber was replaced 2 h after adding GAS, and the Transwell inserts containing the keratinocytes were moved to new wells containing fresh medium every 2 h to prevent overgrowth of translocated bacteria. We assessed translocation by quantitative cultures of medium from the lower chamber at 2 h intervals.

Apligraf living skin equivalent (a gift from Organogenesis) was used as a model for human skin[14]. Samples of skin equivalent were cut into rectangular sections, each approximately 2.5 × 1.2 cm. Each section was placed on a 12 mm Transwell (3.0-μm pore size; Costar) and the Transwell was placed on Todd Hewitt agar containing 5% sheep blood. The apical surface of the skin equivalent was lightly brushed with a sterile cytology brush to abrade the stratum corneum, exposing the underlying epidermal keratinocytes. GAS was resuspended at 10^6 colony-forming units per 10 μl^{-1} in SFM supplemented with 0.3 mM calcium chloride, and inoculated onto the surface of the tissue. After inoculation, we incubated tissue samples at 37 °C with 5% CO_2 and no supplemental humidity. Transwells containing the inoculated tissue samples were transferred to fresh blood agar every 2 h. The blood agar plates were then incubated overnight at 37 °C for enumeration of colony-forming units representing the number of organisms emerging from the basal surface of the tissue.

Received 20 August; accepted 4 October 2001.

1. Schrager, H. M., Albertí, S., Cywes, C., Dougherty, G. J. & Wessels, M. R. Hyaluronic acid capsule modulates M protein-mediated adherence and acts as a ligand for attachment of group A *Streptococcus* to CD44 on human keratinocytes. *J. Clin. Invest.* **101,** 1708–1716 (1998).
2. Cywes, C., Stamenkovic, I. & Wessels, M. R. CD44 as a receptor for colonization of the pharynx by group A *Streptococcus*. *J Clin. Invest.* **106,** 995–1002 (2000).
3. Lesley, F., Hyman, R. & Kincade, P. W. CD44 and its interaction with extracellular matrix. *Adv. Immunol.* **54,** 271–335 (1993).
4. Oliferenko, S., Kaverina, I., Small, J. V. & Huber, L. A. Hyaluronic acid (HA) binding to CD44 activates Rac1 and induces lamellipodia outgrowth. *J. Cell Biol.* **148,** 1159–1164 (2000); erratum *J. Cell Biol.* **149,** 236 (2000).
5. Bourguignon, L. Y. W., Zhu, H., Shao, L. & Chen, Y.-W. CD44 interaction with c-Src kinase promotes cortactin-mediated cytoskeleton function and hyaluronic acid-dependent ovarian tumor cell migration. *J. Biol. Chem.* **276,** 7327–7336 (2001).
6. Rheinwald, J. G. The role of terminal differentiation in the finite culture lifetime of the human epidermal keratinocyte. *Int. Rev. Cytol. Suppl.* **10,** 25–33 (1979).
7. Rheinwald, J. G. Serial cultivation of normal human epidermal keratinocytes. *Methods Cell Biol.* **21A,** 229–254 (1980).
8. Bourguignon, L. Y., Zhu, H., Shao, L. & Chen, Y. W. CD44 interaction with tiam1 promotes Rac1 signaling and hyaluronic acid-mediated breast tumor cell migration. *J. Biol. Chem.* **275,** 1829–1838 (2000).
9. Tsukita, S., Oishi, K., Sato, N., Sagara, J. & Kawai, A. ERM family members as molecular linkers between the cell surface glycoprotein CD44 and actin-based cytoskeletons. *J. Cell Biol.* **126,** 391–401 (1994).
10. Legg, J. W. & Isacke, C. M. Identification and functional analysis of the ezrin-binding site in the hyaluronan receptor, CD44. *Curr. Biol.* **8,** 705–708 (1998).
11. Hall, A. Rho GTPases and the actin cytoskeleton. *Science* **279,** 509–514 (1998).
12. Taher, T. E. *et al.* Signaling through CD44 is mediated by tyrosine kinases. Association with p56lck in T lymphocytes. *J. Biol. Chem.* **271,** 2863–2867 (1996).
13. Parenteau, N. L., Bilbo, P., Nolte, C. J., Mason, V. S. & Rosenberg, M. The organotypic culture of human skin keratinocytes and fibroblasts to achieve form and function. *Cytotechnology* **9,** 163–171 (1992).
14. Sabolinski, M. L., Alvarez, O., Auletta, M., Mulder, G. & Parenteau, N. L. Cultured skin as a 'smart material' for healing wounds: experience in venous ulcers. *Biomaterials* **17,** 311–320 (1996).
15. Finlay, B. B. & Cossart, P. Exploitation of mammalian host cell functions by bacterial pathogens. *Science* **276,** 718–725 (1997).
16. McCallum, S. J. & Theriot, J. A. in *Cellular Microbiology* (eds Cossart, P., Boquet, P., Normark, S. & Rappuoli, R.) 171–191 (ASM, Washington DC, 2000).
17. Ashbaugh, C. D., Warren, H. B., Carey, V. J. & Wessels, M. R. Molecular analysis of the role of the group A streptococcal cysteine protease, hyaluronic acid capsule, and M protein in a murine model of human invasive soft-tissue infection. *J. Clin. Invest.* **102,** 550–560 (1998).
18. Cline, P. R. & Rice, R. H. Modulation of involucrin and envelope competence in human keratinocytes by hydrocortisone, retinyl acetate, and growth arrest. *Cancer Res.* **43,** 3203–3207 (1983).
19. Crowe, D. L., Hu, L., Gudas, L. J. & Rheinwald, J. G. Variable expression of retinoic acid receptor (RARβ) mRNA in human oral and epidermal keratinocytes; relation to keratin 19 expression and keratinization potential. *Differentiation* **48,** 199–208 (1991).
20. Tchao, R. in *Alternative Methods in Toxicology* (ed. Goldberg, A. M.) 271–283 (Ann Liebert, New York, 1988).
21. McNamara, B. P. *et al.* Translocated EspF protein from enteropathogenic *Escherichia coli* disrupts host intestinal barrier function. *J. Clin. Invest.* **107,** 621–629 (2001).

Supplementary Information accompanies the paper on *Nature*'s website (http://www.nature.com).

Acknowledgements

We thank E. Meluleni for preparation of the histology specimens; M. Lowe for assistance with the confocal microscopy; and R. Stearns for assistance with scanning electron microscopy. This work was supported by the National Institutes of Health.

Correspondence and requests for materials should be addressed to M.R.W. (e-mail: mwessels@channing.harvard.edu).

The AAA ATPase Cdc48/p97 and its partners transport proteins from the ER into the cytosol

Yihong Ye*, Hemmo H. Meyer† & Tom A. Rapoport*

** Howard Hughes Medical Institute and Department of Cell Biology, Harvard Medical School, Boston, Massachusetts 02115, USA*
† Department of Cell Biology, Yale Medical School, 333 Cedar Street, SHM C432, New Haven, Connecticut 06520, USA

In eukaryotic cells, incorrectly folded proteins in the endoplasmic reticulum (ER) are exported into the cytosol and degraded by the proteasome[1]. This pathway is co-opted by some viruses. For example, the US11 protein of the human cytomegalovirus targets the major histocompatibility complex class I heavy chain for cytosolic degradation[2]. How proteins are extracted from the ER membrane is unknown. In bacteria and mitochondria, members of the AAA ATPase family are involved in extracting and degrading membrane proteins[3,4]. Here we demonstrate that another member of this family, Cdc48 in yeast and p97 in mammals, is required for the export of ER proteins into the cytosol. Whereas Cdc48/p97 was previously known to function in a complex with the cofactor p47 (ref. 5) in membrane fusion[6–8], we demonstrate that its role in ER protein export requires the interacting partners Ufd1 and Npl4. The AAA ATPase interacts with substrates at the ER membrane and is needed to release them as polyubiquitinated species into the cytosol. We propose that the Cdc48/p97–Ufd1–Npl4 complex extracts proteins from the ER membrane for cytosolic degradation.

We proposed that Cdc48/p97 may have a role in ER protein degradation on the basis of several pieces of indirect evidence. First, Cdc48 binds to Ufd1, Ufd2 and Ufd3 (refs 9–11), which are involved in the degradation of ubiquitin-fusion proteins[12]. Second, a complex of Cdc48, Ufd1 and Npl4 (a protein originally identified in a screen for nuclear transport defects[13]) functions in the proteasome-dependent cleavage of ER membrane proteins that serve as the precursors to two transcription factors (Spt23 and Mga2)[14]. Third, both mammalian p97 and yeast Cdc48 interact with the proteasome and a degradation substrate[15,16]. Finally, a large fraction of both Cdc48 and p97 is associated with ER membrane (ref. 6 and Y.Y., unpublished results).

To test directly the involvement of Cdc48 in ER protein degradation, we analysed the stability of misfolded ER proteins in *CDC48* mutants of *Saccharomyces cerevisiae*. As a membrane protein substrate we choose H–$2K^b$, a major histocompatibility complex (MHC) class I heavy chain that in yeast is quickly degraded in a proteasome-dependent manner[17]. Wild-type or *cdc48-1* mutant cells were pulse-labelled with [^{35}S]methionine at a non-permissive temperature and incubated with unlabelled methionine for different time periods. Cell lysates were subjected to immunoprecipitation with antibodies to H–$2K^b$. The results showed that H–$2K^b$ was much more stable in *cdc48-1* mutant than in wild-type cells (Fig. 1a). A significant stabilization of H–$2K^b$ was seen with another *CDC48* mutant (*cdc48-3*), even at permissive temperature (Fig. 1b).

We tested the misfolded lumenal protein CPY*, an aberrant form of carboxypeptidase Y (CPY), which is degraded by the ubiquitin-proteasome pathway[18]. The stability of CPY* was analysed by immunoblotting after inhibition of protein synthesis with cycloheximide. Whereas CPY* was rapidly degraded in wild-type cells at both 30 °C and 23 °C, the protein was significantly more stable in *cdc48-1* cells (Fig. 1c), particularly at 23 °C—the restrictive temperature for the mutant. The half-life of CPY* was also increased in